ranger – a Pattern Recognition Algorithm for the HERA-B Main Tracking System

Part I: The HERA-B Pattern Tracker

Rainer Mankel
Humboldt University Berlin, Germany

April 24, 1997

Abstract

A pattern recognition strategy for the HERA-B main tracking system is presented. A *concurrent track evolution* algorithm has been developed to select the optimal track candidate compatible with a seed. Intrinsically a local method, it combines the virtues of track following procedures with the necessary ability to optimize between many available paths in a high occupancy environment. The problem of hit-location in a multiplanar detector geometry is solved with an approach called *domain navigation*. This note gives a detailed description of the algorithm and shows its performance, which has been evaluated using HERA-B Monte Carlo events with full detector simulation and the current spectrometer geometry implementation, which is already quite realistic.

1 Introduction

The HERA-B detector [1] has been designed to take full advantage of the abundant $b\bar{b}$ cross section in energetic pN collisions and the huge Lorentz boost under which the B mesons are produced. The requirements to measure CP violation resulted in a forward spectrometer geometry. This setup has a number of consequences for the design of the tracking system:

- The large track density and the high bunch crossing frequency require fast and highly granular tracking devices.
- The strong radial dependence of the track density and the necessity of matched granularities require the combination of different detector technologies. The suitable tracking options, as honeycomb drift chambers

(HDC), micro strip gaseous chambers (MSGC), scintillating fibres or silicon microstrip detectors introduce considerable amounts of material into the tracking area.

- The necessity to keep the cell occupancy at a reasonable level with drift chamber technology require separating wires into several sections. All this leads to a complicated *multiplanar* tracker geometry.

- In contrast to cylindrical spectrometer layouts with a solenoidal field encompassing the whole tracking volume, forward spectrometers with a limited, instrumented magnet area have to cope with an inhomogeneous field. Since the field is also not unidirectional, pattern recognition in the field has to deal with five track parameters simultaneously, which in a high track density may become a hopeless task, especially since spiralling low-momentum particles will contribute considerably to the occupancy.

The general concept of track reconstruction in the HERA-B spectrometer [3, 4] is shown in fig. 1. This figure also shows the coordinate system used throughout this note: the origin is located at the target position, the z axis points in the direction of the proton beam, the x axis is oriented normal to z in the horizontal plane, and the y axis is directed such that (x, y, z) form a right-handed system. The main bending component of the magnetic field points is approximately parallel to the y direction. The spectrometer is divided into a *vertex detector* employing silicon strip technology for precision measurement of vertices, and a *main tracker* dedicated to momentum measurement, K_S^0 vertex detection and triggering. Most importantly, the main tracker contains tracking devices behind the magnet but in front of the RICH, where the stray magnetic field is low enough (< 50 Gauss) to allow for straight-line track finding. This area is called the *pattern tracker*, since it is used for the initial stage of pattern recognition. It consists of four superlayers of inner and outer tracker, sufficient for standalone pattern recognition, and has been placed intentionally upstream of the RICH which represents a source of secondary particles created in its gas volume and mirror system. As described in more detail below, track segments found in the pattern tracker are propagated through the magnet, determining the particle's momentum, an estimate of which is already given by the track deflection relative to the direction to the target. The resulting track is then continued upstream through the vertex detector, and downstream to the lepton identification devices. Two additional tracker superlayers behind the RICH are mainly used by the first level trigger. They also serve together with the pattern tracker to provide an excellent measurement of the track's position and direction in the RICH.[1]

Also the silicon vertex detector (SiVD) can be used for initial track finding [5]. Though its geometrical acceptance for long-lived particles like the K_S^0 is limited,

[1]As the spectrometer of the proposed LHC-B experiment [2] has in many aspects a similar layout, the method developed here is likely to be also applicable for LHC-B.

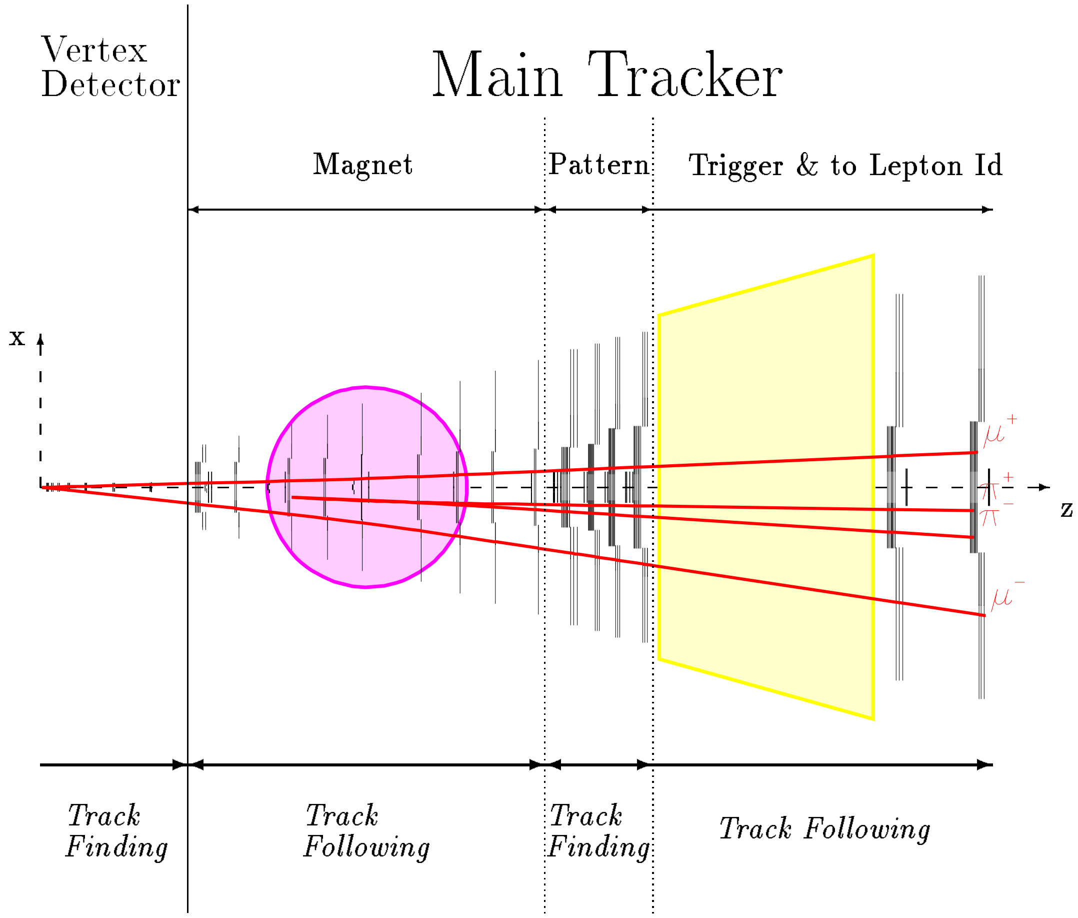

Figure 1: Layout of the HERA-B vertex and main tracking system (top view). The proton beam enters from the left side. The tracking areas used for track finding and track propagation (see text) are indicated at the bottom. The shaded areas are the pole shoes of the magnet (left) and the RICH (right). Only the track finding in the *pattern tracker* is subject of this note.

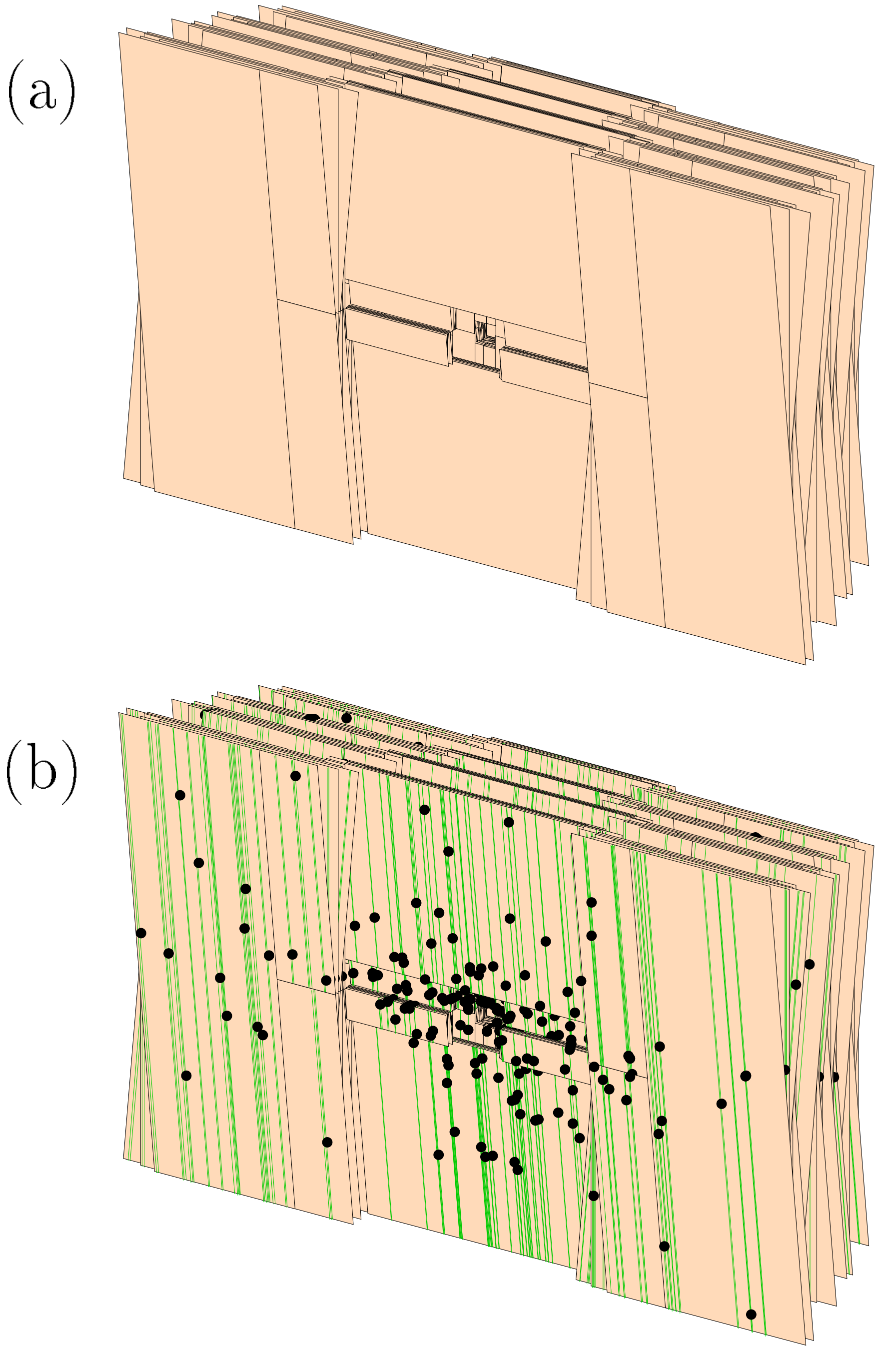

Figure 2: Isometric view of the HERA-B pattern tracker (a) as it is implemented in the HERA-B geometry description. The subdivision of each layer into 12 sectors of the outer tracker and eight sectors of the inner tracker is visible. In (b) a typical simulated event is displayed, indicating the firing wires and strips.

it provides additional redundancy for track finding. This note concentrates on track finding in the pattern tracker.

In order to match the granularity to the track density, HERA-B uses honeycomb drift chambers (HDC) for the outer and special highly granular devices for the inner tracker. Micro-strip gaseous chambers (MSGC) and scintillating fibres are the main options for the inner tracker. The diameter of the honeycomb drift chamber cells is 10 mm for the outer and 5 mm for the inner sectors. Each of the outer tracker layers is subdivided into 12 sectors to adjust the channel count to the track density. The inner tracker layers are assumed to be divided into four corner-shaped modules, each of which is logically composed of two rectangle-shaped sectors.

An isometric view of the *multiplanar geometry* of the pattern tracker as it is implemented in the HERA-B geometry description is shown in fig. 2a. It consists of four superlayers of outer and inner tracking devices. Each superlayer consists of six individual layers, except for the second and third inner tracker superlayers which have only four layers. In half of the layers, the wires are exactly vertical, these will be referred to as the 0° layers, the other half are *stereo layers* with the wires and strips tilted by approximately ± 100 mrad. In the first and fourth superlayer, one layer of each orientation is designed as a double layer to provide high efficiency for first level trigger which uses these layers. A typical simulated event in the bottom half (fig. 2b) shows the hit density prevalent in normal HERA-B running conditions. Both pictures have been generated with version 4.7 of the event visualization tool *prism* [6].

The use of drift chamber technology in spite of the large track density results in high cell occupancies, which in the case of HERA-B range up to 20% in the pattern tracker and may be even higher in the magnet tracker. While in traditional tracking systems, overlap of tracks is relatively rare, the HERA-B tracker must cope routinely with clusters of hits from nearby tracks. This challenge is further enhanced by the fact that the drift chamber cell size is very small (5 and 10mm), making resolution of the left-right ambiguity particularly difficult. Additional ambiguities are introduced since the first tracking step uses only the 0° layers, thus is ignorant of the y coordinate and cannot discern which of the vertically stacked layer sectors contains the next proper hit. Another source of ambiguity arises from the hit inefficiency (assumed 5% for the inner and 2% for the outer tracker) together with the limited double hit resolution (assumed values 800 μm for the inner tracker, 5mm and 10mm cell size for HDC). Pattern recognition does not only have to cope with missing or unusable hits ('faults') in a layer, but also with the possibility that a seemingly matching hit contains wrong information which will misguide further track propagation.

The complicated geometrical pattern in the *multiplanar geometry* of the HERA-B main tracker poses another problem for pattern algorithms, since eg. locating the next suitable detector hit on a trajectory becomes a nontrivial task. We will refer to this problem as *navigation*. Navigation strategies have to ensure that no hits are missed on relevant tracks, while on the other hand reducing the effort spent on hit-checking to a minimum. A *navigation strategy* suitable for the HERA-B spectrometers, called *domain navigation*, which can be effectively embedded in the concurrent track evolution concept will be explained below.

2 The Concurrent Track Evolution Strategy

Pattern recognition in hadronically produced B events in areas of high occupancy is bound to fully exploit the constraints of an underlying track model (a comparison to a methods without track model can be found in [7]). *Local methods* of pattern recognition – also referred to as *track following methods* – provide a natural way of using the information of the track model, since they start with a *seed*, ie. an initial guess of a track candidate and follow its presumed trajectory through the sensitive detector volume, collecting hits compatible with this trajectory along the way. While this method is relatively easy to apply to tracking scenarios with moderate track density and often leads to a reasonable computational effort since the number of hits to be considered is roughly proportional to both the number of layers and the number of tracks, the application to situations with large hit density is not straight-forward. In dense environments, track following runs the risk of losing its trail whenever several possible continuations exist. The main complications can be summarized as follows:

1. wrong hits with lower χ^2 than proper hits
2. missing hits
3. wrong hits replacing missing hits
4. left/right ambiguities in wire drift chambers

These aspects can pose a particular problem if the track density is subject to strong variations, as is the case at HERA-B due to the fluctuating number of simutaneous interactions during one bunch crossing.

The concurrent track evolution strategy has been developed with the intention to provide a general approach to evaluate the *available paths* for a track candidate *concurrently* to find an optimal solution, while at the same time keeping the combinatorics at a reasonable level. Since branching into several paths will in general occur at any level, the algorithm has to be set up such that it can handle any number of candidates in parallel. On the other hand, the growth of the number of track candidates with increasing hit density can become a huge problem when events of varying interaction multiplicity have to be reconstructed on a processor farm. The concurrent track evolution handles this problem by optimizing the population of track candidates in each evolution step, using quality estimators for relative and absolute cuts on the track quality. As will be shown in

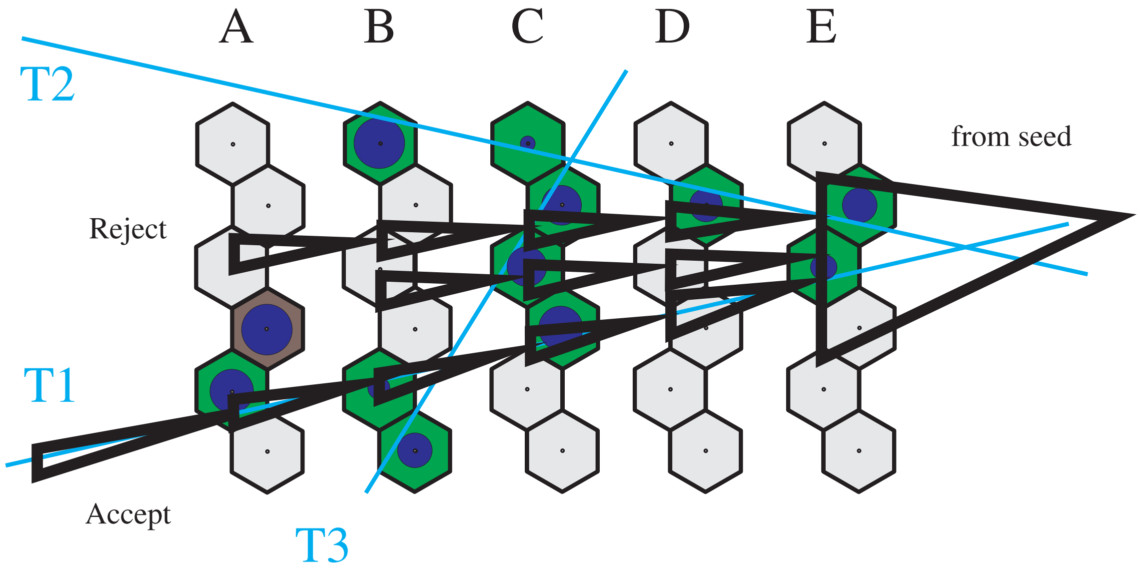

Figure 3: Illustration of the concurrent track evolution strategy for an ambiguous situation caused by three nearby tracks in a superlayer of the HERA-B outer tracker. The propagation proceeds upstream from the right to the left. We assume that the propagation started with a seed of hits from track T2.

the following, this approach leads to a favourable timing behaviour towards high multiplicity events. The concurrent track evolution strategy can also be regarded as a variant of *deferred arbitation* (see [8]). The idea of this strategy is illustrated in fig. 3, which shows a potentially ambiguous situation caused by two nearby tracks T1 and T2 plus a large angle track T3 in five layers of honeycomb drift chambers. The simulated drift time isochrones are indicated by circles. For simplicity, we assume here that the algorithm discards track candidates with more than one missing hit (*fault*) in a row, and that the maximum population size is three. We also assume that a seed of hits from track T2 has been formed on the right side outside of the figure. The propagation proceeds upstream from right to left. The predicted coordinate from the seed is compatible with four coordinates originating from two HDC hits in layer E. Since the population is limited to three simultaneous candidates, the best choices give rise to three new three new candidates, while the least favourable uppermost coordinate is discarded. In the propagation to layer D, only the uppermost candidate finds a suitable hit, since track T2 did not produce a hit in this layer, e.g. due to layer inefficiency. In layer C, all three candidates absorb an additional hit. In layer B, the middle candidate is discarded, since its quality – diminished by two faults and two *wrong* hits – is too low compared to the successful lower candidate. In layer A, the uppermost candidate is discarded because its two subsequent faults exceed the limit, so that only the correct candidate remains.

Track following in the strict sense would always accept the hit with the smallest χ^2 contribution, possibly a good solution when the hit density is small. In the presence of multiple scattering and high hit density, a wrong hit will frequently have a smaller χ^2 contribution than the proper one, or *replace* a proper hit which is missing due to detector inefficiency, or be destroyed by another track passing the same cell. On the other hand, full evaluation of all possible hit combinations would exceed all bounds of computing resources when applied to dense events. Thus, the concurrent track evolution strategy combines the virtues of track following and combinatorial approaches. As will be shown below, the optimization in each evolution step using a quality estimator provides an elegant means to deal with the main problems in high occupancy track propagation.

3 Implementation for HERA-B

3.1 Pattern Recognition Concept

The tracks in the HERA-B main tracking system can be described by a set of five track parameters: impact parameters x_0 and y_0, the *direction tangents* (*slopes*) $t_x = \tan\theta_x$ and $t_y = \tan\theta_y$ and a momentum-related parameter, e.g. the inverse momentum signed according to charge, Q/p, all taken at a reference z position (z_0)[2]. The general concept developed for HERA-B seeks to *factorize* the pattern recognition process into three passes such that only $1-2$ track parameters have to be handled at a time.

1. The first pass finds straight track candidates in the xz projection processing only the hit information from the 0° layers of the *pattern tracker* downstream of the magnet. In this area, the residual magnetic field strength is < 50 Gauss, so that the straight line parametrization is valid within the tracker resolution for the relevant tracks. This pass determines the track parameters x_0 and t_x at a reference position z_0.

2. The second pass finds the corresponding *vertical* track candidate in the yz projection using simultaneously the hit information from the $\pm5°$ stereo layers. Since the hit coordinates measured by the stereo layers (u) are defined by the relation

$$u = x\cos\alpha_{\mathrm{st}} - y\sin\alpha_{\mathrm{st}}$$

where α_{st} is the stereo angle, the measured stereo coordinates are converted to y coordinates by using the track's known xz projection:

$$y = \frac{(x_0 + t_x(z - z_0))\cos\alpha_{\mathrm{st}} - u}{\sin\alpha_{\mathrm{st}}}$$

[2]During the track propagation, the z position of the current hit is taken as reference

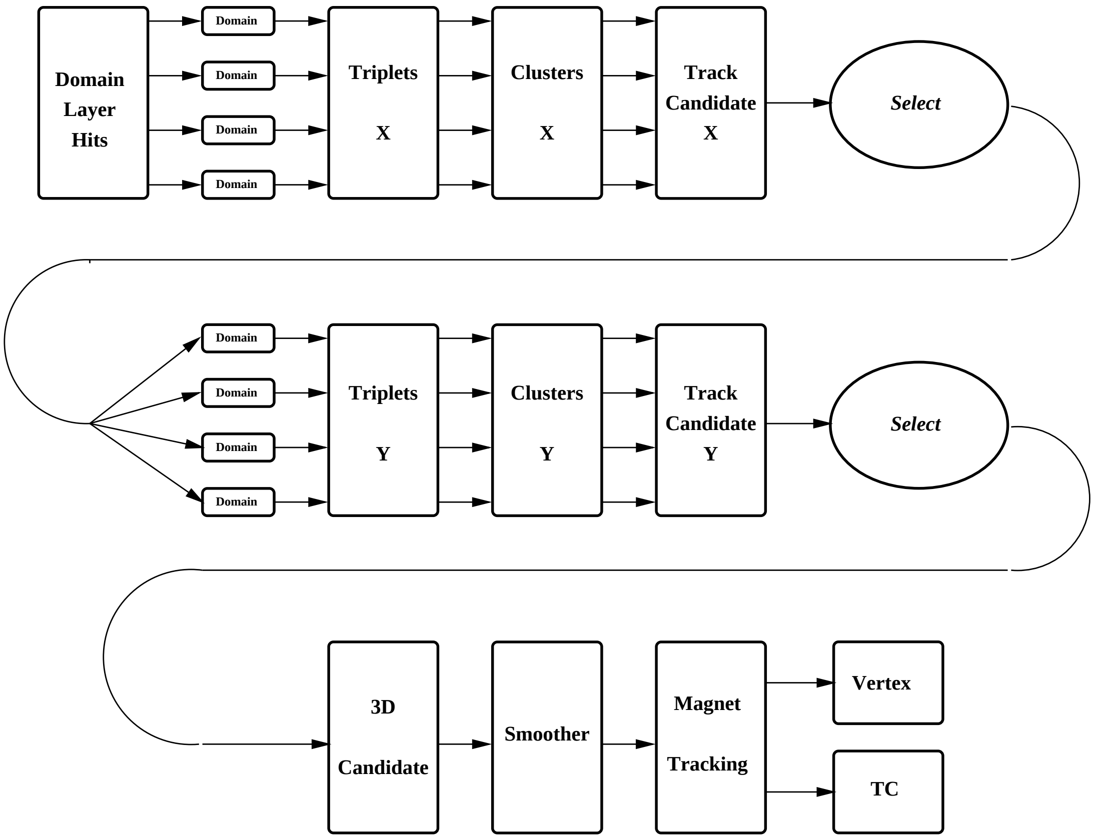

Figure 4: Flow chart representing the *ranger* tracking concept. Magnet tracking and continuation to vertex detector and trigger chambers are not discussed in this note.

After the vertical track candidate has been found, its hits are combined with those of the xz projection, and a three-dimensional track candidate is fitted.

3. In the third pass, which will be the subject of another HERA-B note, this three-dimensional track candidate is propagated through the tracker inside the magnetic field, determining the particle's charge and momentum.

The various steps of the *ranger* tracking concept are shown in a flow diagram in fig. 4 and will be described in the following sections.

3.2 The Triplet Seeding Strategy

Efficient initialization (*seeding*) of track candidates is essential to keep the number of wrong trails followed to the necessary minimum. On the other hand, care must be taken not to sacrifice efficiency already in the seeding process, since

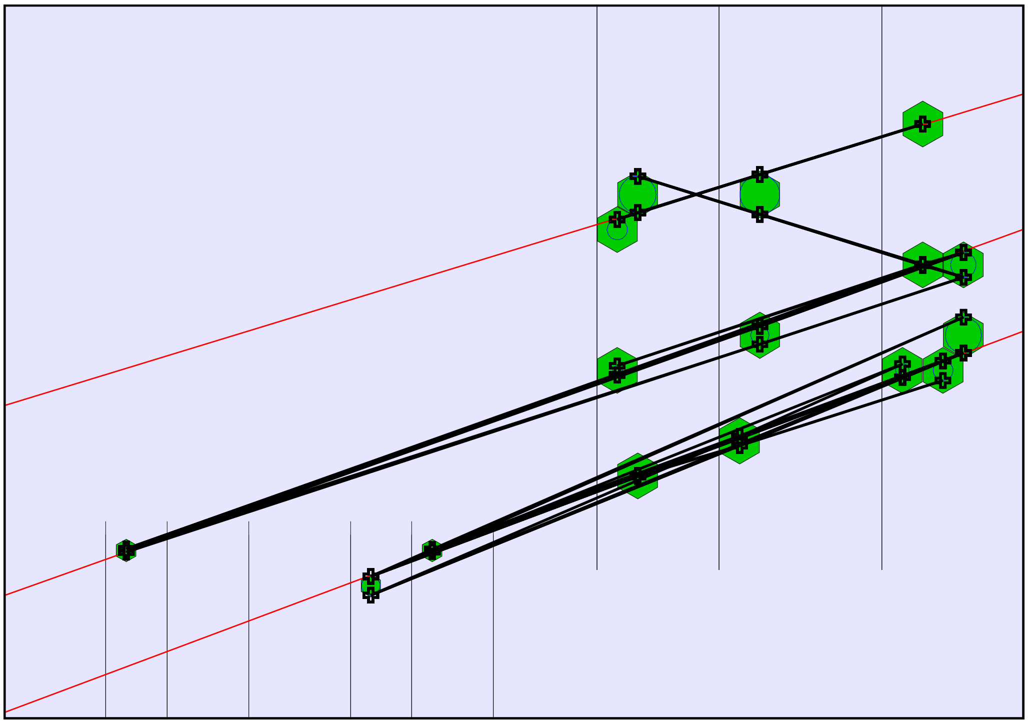

Figure 5: Construction of triplets in the transition area between 5 mm and 10 mm honeycomb cells in the HERA-B outer tracker. The triplets are displayed as thick lines with crosses denoting the hits coordinates which have been used. The thinner lines are the Monte Carlo particles which caused the hits.

tracks lost here are unlikely to be regained in a later stage. In principle a hit *doublet* is sufficient to seed a track candidate in one projection. However, in particular the drift devices in the outer tracker with their left-right ambiguity would yield an enormous number of hit doublets, most of them unsuitable for initializing a proper track. In this work, therefore, hit *triplets* are used to initialize a track candidate. The triplet requirement removes most of the combinations with wrong left-right assignments. This technique is well suited to HERA-B because the pattern tracker superlayers have at least three layers in the zero and stereo projection, with the exception of the second and third inner tracker superlayers.

Triplets are formed from two doublets which share a common hit if their directions agree within $\mathrm{N}^{\mathrm{max}}_{\sigma,\mathrm{triplet}}$ times the resolution. Only doublets with $\tan\theta < 1$ are accepted. The mean probability to find a proper triplet in the 0° projection for a reference track is 96.8% if only the hindmost superlayers of inner and outer tracker are used. For the studies in this note, both the first and last superlayers were used for triplet seeding. In this case, the combined triplet efficiency is already 99.7%. It may still be useful to employ also the middle superlayers for triplet search to compensate for temporary module failures in real data taking.

Figure 5 shows the assignment of triplets in a closeup from the HERA-B outer tracker.

The number of proper triplets for a given particle can be as small as one (or zero in case of faults) and larger than 20 in sector overlap areas. To reduce the number of candidates, the triplets are clustered if they are closer than $\delta \mathrm{x}_{\mathrm{clus}}^{\mathrm{max}}$ in the measured coordinate[3] and $\delta \mathrm{t}_{\mathrm{x,clus}}^{\mathrm{max}}$ in slope, before they are subjected to track propagation.

3.3 Domain Navigation in a Multiplanar Detector Geometry

A central issue relevant for the speed of a track following algorithm is the effort needed to identify potential subsequent hits for the continuation of a track candidate. This procedure will here be referred to as *navigation*. In highly symmetric detector geometries like e.g. a cylindrical drift chamber, navigation seldom poses a particular problem since the next drift cell traversed by the particle can usually be related to the layer number and the predicted impact point through a simple formula. The HERA-B main tracker consist of thousands of individual detector modules with different shapes, granularities and wire/strip lengths which are arranged in a complicated three-dimensional pattern. Data acquisition and event building group the hit information according to modules. The task of locating hits in a given direction is complicated by the fact that

- while the HERA-B layers as a whole are almost *hermetic*, this is only reached through generous overlap of sectors with some distance in z,
- the stereo layers and the 0° layers do not cover exactly the same area in the xy plane, and
- the vertical coordinate is unknown during track following in the 0° projection.

The main goals for a HERA-B navigation strategy were:

- to integrate inner and outer tracker devices into a common concept,
- to make possible the full exploitation of layer hermiticity for pattern recognition,
- to minimize the number of hits to be checked in a single propagation step,
- to provide a universal solution for track propagation in three dimensions as well as in both projections,

[3] sampled at a mean z reference coordinate for the domain window

Domain	Outer tracker superlayer	Inner tracker superlayer
PC1	PC01	MS10
PC2	PC02	MS11
PC3	PC03	MS12
PC4	PC04	MS13

Table 1: Pattern tracker domains and the superlayers assigned to them. The domain names are derived from the names of the outer tracker superlayers.

- to limit the use of lookup tables to the navigation between the superlayers, and
- to keep the amount of memory used by navigation tables on a reasonable level.

The solution developed for the HERA-B main tracker is based on defining *virtual* devices with a geometry simpler than the real one. Corresponding superlayers of inner and outer tracking are combined to new logical entities called *domains*. The HERA-B pattern tracker is hence represented by four domains. The assignment of superlayers to domains is displayed in table 1. In each domain, *windows* are defined which comprise tracking channels of similar granularity and length. Their borders are parallel to the x and y axes. Each domain window contains several *domain layers*. Each domain layer is assigned to all suitable wires and strips which are completely or partly contained in the domain window. This means that measurements inside a domain layer are not limited to a single z value. Another consequence is that stereo hits at the window borders can belong to more than one window.

The assignment of detector channels to domain windows is illustrated in fig. 6a–d. Figure 6a displays the *logical* window structure of the upper middle part of the outer tracker, which is similar to the detector sections of the 0° chambers. The numbers indicate the official detector section numbering as defined in [3]. These windows roughly group detector modules of comparable size and pitch. The role of the window above the beam is illustrated in figs.6b and 6c, which show how the outer tracker may be built from standard size modules[4]. Figure 6b shows a 0° layer, where the modules with channels belonging to the window have been emphasized by a lighter shade. Figure 6c shows a +5° layer, built from standard modules rotated by this angle. The shaded areas show how modules from neighbouring sectors are used to create a hermetic logical tracking unit for the same window. This simplification of the spectrometer's geometry is bought at the expense that some hits may belong to several windows and, since

[4]Since this full module structure is not yet implemented in the geometry definition of the HERA-B detector simulation, larger, epiped shaped detector planes have been used for the quantitative studies described below

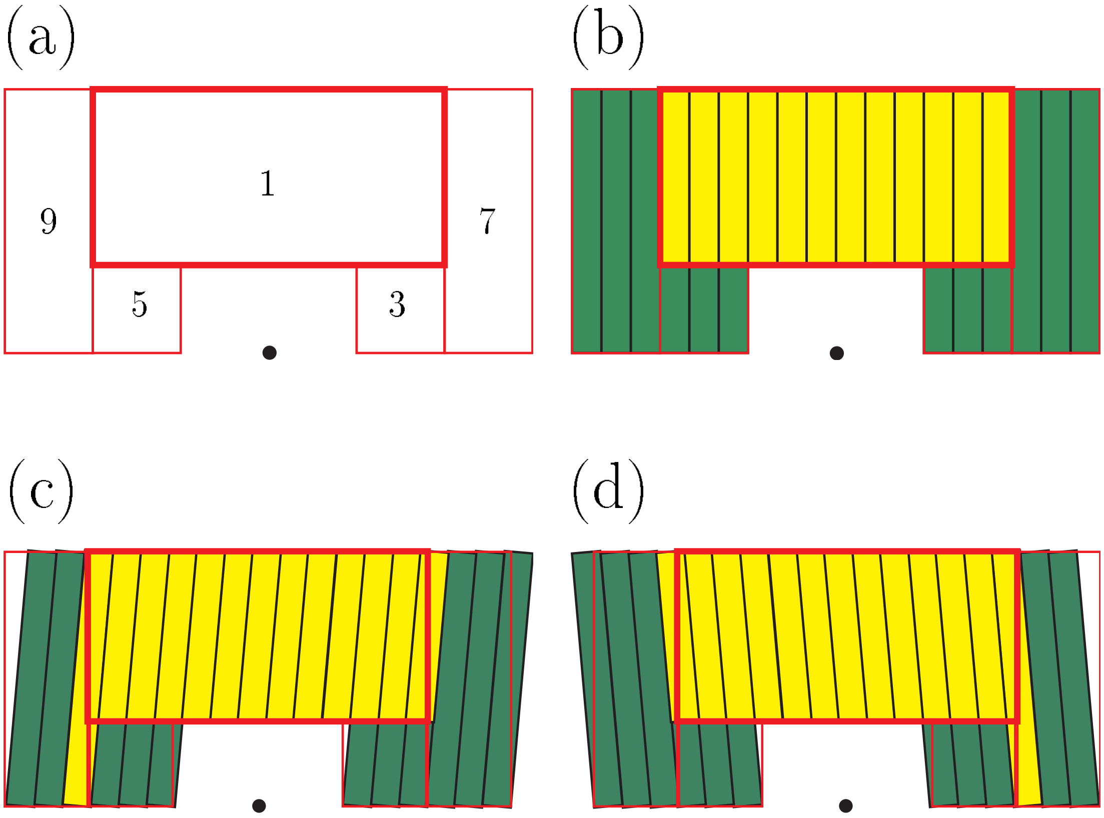

Figure 6: Illustration of the assignment of detector channels to domain windows in the upper middle part of the HERA-B outer tracker. The beam position is indicated by a point. For clarity, the inner tracker as well as the other outer tracker planes have been omitted. (a) Structure of the *logical* windows, (b) assignment of detector standard modules to the domain window labelled '1' in a 0° layer, assigned modules denoted by lighter shading, (c) similar for a 5° stereo layer, and (d) for a -5° stereo layer.

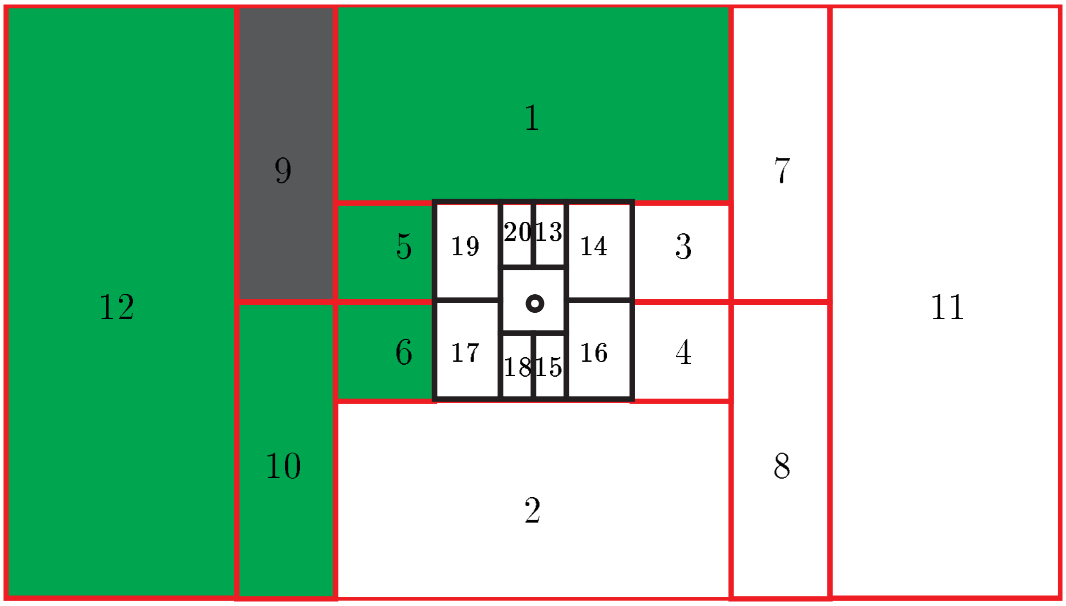

Figure 7: Example for the navigation options of a selected domain window (dark texture) when navigating from one domain to the next. The domain windows with lighter shade are included in the navigation table as *target windows*. Note that only the topology of the domain window structure is displayed, the relative proportions of the windows are not to scale.

neighbouring plane sectors may be at different z values, the hit sequence may become partially reversed, leading to complications in the multiple scattering treatment.

The navigation proceeds according to the following scheme:

1. A track candidate is seeded in a particular domain window.

2. Within the same domain, the propagation is restricted to the same window. The domain window borders are designed with sufficient overlap.

3. When going from one domain to the next, a lookup table provides a list of domain windows to which the track propagation may proceed. An example is given in fig. 7.

4. The procedure is repeated until no further navigation options are available, e.g. at the end of the spectrometer, or all track candidates have been discarded (see next section).

Each track candidate passing all four domains is thus characterized by the four domain windows which it passes. This knowledge is used in the second track finding step which looks for the yz projection of the track. The search for stereo layer hits for both seeding and propagation is restricted to hits belonging to these domain windows.

The list of domain windows available for navigation is derived from a navigation table based on domain sectors. The domain sectors are numbered consecutively within a domain. They are related but not identical to the GEDE sectors in *Arte's* GEDE table, since the GEDE sectors are numbered individually in each type of hardware component, which would lead to name clashes within the same domain. The assignment of domain sector numbers is indicated in fig. 7. (The numbering of GEDE sectors for the outer tracker can be found in [3], p. 236.) The navigation table used for the quantitative studies below is listed in table 2. This table shows also the relation between the domain sector and GEDE sector numbering schemes.

3.4 Implementation of the Concurrent Track Evolution Strategy

After one or several seeds have been selected, a recursive growth procedure is applied. All track candidates have a status flag which may be 'alive', 'mature' or 'dead'. Initially, the seed(s) are marked as 'alive'. In each evolution step, each candidate is branched to all valid navigation target windows. In each window, the predicted coordinate is calculated, and the algorithm branches to all hits within a range of $\pm\delta_{\mathrm{u}}^{\mathrm{max}}$ around this prediction. For each valid hit – including both left/right assignments for drift distance measurements – the filter step (see below) is invoked, giving *birth* to a new track candidate. If the filtered χ^2 contribution of this hit exceeds a limit ($\delta\chi^2_{\mathrm{max}}$), the branch is discarded. To account for missing hits (faults), also the original candidate re-enters the growth cycle without a new hit, with the counter of subsequent faults increased by one, provided the maximum number of subsequent faults ($\mathrm{N}_{\mathrm{Faults}}^{\mathrm{max}}$) is not exceeded.

The rapid growth of the number of track candidates is regulated at the end of each evolution step by imposing absolute as well as relative cuts. For each new development branch, a quality measure is calculated. The 'quality' of a candidate could be a very general estimator function like:

$$Q = f(\mathrm{N}_{\mathrm{Steps}}, \mathrm{N}_{\mathrm{Faults}}, \chi_i^2, x, y, t_x, t_y, ...)$$

where $\mathrm{N}_{\mathrm{Steps}}$ is the number of evolution steps carried out so far. For the results shown in this note, the following, relatively simple estimator turned out to work

Domain sector	Device	GEDE sector	navigation targets (domain sectors)
1	PC	1	1, 9, 7, 3, 5, 19, 20, 13, 14
2	PC	2	2, 8, 10, 4, 6, 17, 18, 15, 16
3	PC	3	3, 7, 14, 4, 1
4	PC	4	4, 8, 16, 3, 2
5	PC	5	5, 9, 19, 6, 1
6	PC	6	6, 10, 17, 5, 2
7	PC	7	7, 1, 3, 11, 8, 4
8	PC	8	8, 2, 4, 11, 7, 3
9	PC	9	9, 1, 5, 12, 10, 6
10	PC	10	10, 2, 6, 12, 9, 5
11	PC	11	11, 7, 8
12	PC	12	12, 9, 10
13	MS	1	13, 14, 20, 1
14	MS	2	14, 3, 13, 1, 20, 16, 4
15	MS	3	15, 16, 18, 2
16	MS	4	16, 4, 15, 2, 18, 14, 3
17	MS	5	17, 6, 18, 2, 15, 19, 5
18	MS	6	18, 15, 17, 2
19	MS	7	19, 5, 20, 1, 13, 17, 6
20	MS	8	20, 13, 19, 1

Table 2: Skeleton of the navigation table used in the HERA-B pattern tracker. The term *GEDE sector* refers to the sector numbering in stored in the Arte GEDE table.

Parameter	Value	Parameter	Value
$\mathrm{N}^{\mathrm{min}}_{\mathrm{Hits}}(\mathrm{x})$	9	$\delta^{\mathrm{max}}_{\mathrm{u}}$	3 cm
$\mathrm{N}^{\mathrm{min}}_{\mathrm{Hits}}(\mathrm{y})$	9	w_{χ^2}	0.1
$\delta\chi^2_{\mathrm{max}}(\mathrm{x})$	8	$\delta\mathrm{q}_{\mathrm{min}}$	-1
$\delta\chi^2_{\mathrm{max}}(\mathrm{y})$	16	$\mathrm{N}^{\mathrm{max}}_{\sigma,\mathrm{triplet}}$	2
$\mathrm{N}^{\mathrm{max}}_{\mathrm{Faults}}(\mathrm{x})$	2	$\delta\mathrm{x}^{\mathrm{max}}_{\mathrm{clus}}$	0.06 cm
$\mathrm{N}^{\mathrm{max}}_{\mathrm{Faults}}(\mathrm{y})$	2	$\delta\mathrm{t}^{\mathrm{max}}_{\mathrm{x,clus}}$	0.02
$\mathcal{R}_{\mathrm{max}}$	5		

Table 3: Table of parameters used in the HERA-B implementation

sufficiently well:

$$Q = \mathrm{N}_{\mathrm{Steps}} - \mathrm{N}_{\mathrm{Faults}} - w_{\chi^2} \times \sum_i \chi_i^2$$

with $w_{\chi^2} = 0.1$. This implies that a fault reduces the quality by 1 unit with respect to a non-faulty track in the same generation. A fault is equivalent to a badly-matching hit with a χ^2 contribution of 10. In addition, relative cuts are placed in each evolution step on the quality difference to the best candidate

$$Q - Q_{best} \geq \delta\mathrm{q}_{\mathrm{min}}$$

with $\delta q_{min} = -1$ in this study. Finally, it is useful to limit the total number of candidates allowed in parallel. If a relative rank $\mathcal{R}$ is assigned to each candidate, with $\mathcal{R} = 1$ indicating the candidate with the highest value of Q, the requirement

$$\mathcal{R} \leq \mathcal{R}_{max}$$

ensures that only the $\mathcal{R}_{max}$ best candidates are kept in each growth cycle ($\mathcal{R}_{max} = 5$ in this work).

If a track candidate is discarded from further propagation, its status flag is changed. If the candidate satisfies requirements for a final track candidate, presently only a requirement on the number of hits

$$\mathrm{N}_{\mathrm{Hits}} \geq \mathrm{N}^{\mathrm{min}}_{\mathrm{Hits}}$$

its flag is set to 'mature', otherwise it is flagged as 'dead' and ignored for all further issues. The growth procedure is terminated when no 'alive' candidates remain. In a final step, the best 'mature' candidate derived from this seed is selected. At this stage, one could acount for remaining ambiguities to be resolved in a subsequent tracking step by allowing more than one candidate to be finally selected. For example, one could select several candidates from the 0° projection and subject them to completion in the stereo projections before finally selecting the best one. This refinement turned out to be unnecessary for the studies discussed in the following. The algorithm parameters used for HERA-B are summarized in table 3.

3.5 Application of the Kalman Filter Technique

The above strategy needs the best possible track parameter estimate after addition of each new point. This can be provided with the least computational effort by applying the Kalman Filter method. The Kalman filter technique operates in the following way:

Prediction Using the known track parameters and their covariance matrix from the current step, the coordinate in the next traversed detector layer and its error is calculated using the track model. Hits in the prediction window are selected.

Filter The coordinate of a measured hit is used to update the track parameters and their covariance matrix. Also the χ^2 contribution of this hit to the fit is computed, which is used for calculating the quality estimator discussed in the previous section. This process is called *filtering*. The last filter step always comprises the information of all previously filtered points.

Smoother Propagates the information from the last filtered points backwards again, making the full information from all points available at each point of the trajectory.

From the mathematical point of view, the Kalman filter is a least squares fit done in a progressive, iterative manner. Detailed descriptions of this method can be found in the literature [9, 10]. For this work, the Kalman Filter was implemented using the *gain matrix formalism*. Since all measurements are one-dimensional, matrix inversion is necessary neither in the prediction nor in the filter stage. Multiple scattering is included as process noise, where the momentum value needed to estimate the contribution to the predicted covariance matrix is estimated from the apparent deflection by the magnetic field using the formula

$$p_\perp = |q \int B_y d\ell \times \frac{z_{magnet} - z_{target}}{x_0 - (z_0 - z_{target}) \tan\theta_x}|$$

where $\int B_y d\ell$ is the average field integral of the main bending component, q the particle's charge, z_{magnet} and z_{target} are the z coordinates of magnet center and target and x_0 and θ_x are the impact parameter and track angle of the seed at z_0 in the bending plane. A more detailed description of the Kalman filter implementation for HERA-B can be found in [11].

4 Performance

4.1 Program Versions and Event Sample

The results presented here are valid for the *ranger* version 4.6, which was implemented under Arte version 4.3 [12]. The MSGC variant of the inner tracker was used. The performance of the method was studied using simulated samples of 302 $pAl \to B^0 + X$, $B^0 \to J/\psi K^0_S \to (\ell^+\ell^-)(\pi^+\pi^-)$ interactions and 1200 unbiased inelastic pAl interactions. The interactions were generated using a combination of the PYTHIA 5.7 and FRITIOF 7.0 generators [13]. The events were passed through the full HERA-B detector simulation HBGEAN [14] version 4.1. The default digitization assumes hit efficiencies of 98% and 95%, and Gaussian coordinate resolutions of 200 μm and 80 μm for the outer and inner tracker devices, respectively. If two or more tracks hit the same honeycomb cell, one hit is generated with a drift distance defined by the track closest to the wire. In the inner tracker, two tracks are merged into the same hit if their measured coordinates are closer than a double hit resolution of 800 μm.

4.2 Definition of performance estimators

A large fraction of the particles generated in the simulation are produced by secondary interactions like bremsstrahlung and photon conversion. Most of those are irrelevant to the physics analysis. Hence, pattern recognition efficiencies are calculated for *reference tracks*, which are selected to define the geometrical acceptance as well as the range of physics interest for the experiment. Reference tracks are all charged particles, excluding $e^\pm$ from photon conversions, with a momentum of $p > 1$ GeV, which pass more than 17 layers (out of the possible 24) of the pattern tracker. A reconstructed track is *assigned* to a generated particle if at least 70% of its hits have been caused by this particle. A generated particle is regarded as *found* if it has been assigned at least one reconstructed track. The pattern recognition efficiency is then defined as

$$\epsilon_{\mathrm{PR}} = \frac{\text{Number of reference tracks (found)}}{\text{Number of reference tracks (total)}}$$

A reconstructed track is called a *ghost* if it is not assigned to any generated particle. A relative ghost rate can be defined as

$$\epsilon_{\mathrm{GH}} = \frac{\text{Number of ghosts}}{\text{Number of reference tracks (total)}}$$

4.3 Geometrical acceptance

The number of layers passed by a track has naturally a strong dependence on the particle's rapidity. Figure 8 shows the number of leptons from the golden B decay as a function of pseudorapidity η and the number of layers passed. Inside the rapidity plateau region of the leptons, nearly all leptons pass ≥ 24 layers. In the overlap area of inner and outer tracker around $\eta \approx 4.5$, even higher counts are possible. The clusters visible at low and high rapidity and $N_{\mathrm{Layers}} \approx 0$ correspond to leptons which pass outside the spectrometer's opening

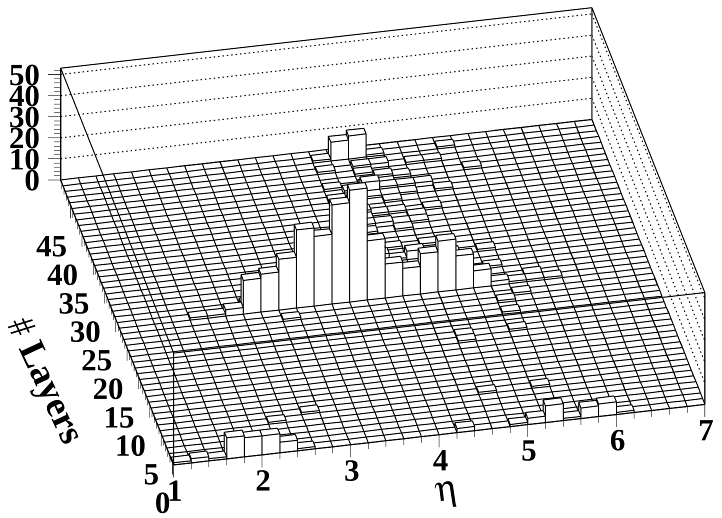

Figure 8: Number of leptons from the golden B decay as a function of pseudorapidity η and the number of layers passed in the pattern tracker. The rapidity is calculated from the momentum vector at the J/ψ decay vertex in the laboratory frame. The distribution shows that within the rapidity range of 2.5–5, almost all leptons from the golden B decay pass at least 24 layers. In the overlap areas of inner and outer tracker around $\eta \approx 4.5$, higher counts are possible. At higher or lower rapidity, an increasing number of particles passes outside the inner or outer acceptance borders so that $N_{\mathrm{Layers}} \approx 0$.

angle or through the beam pipe opening without being detected. Apparently, the requirement $N_{\mathrm{Layers}} > 17$ for reference tracks gives a very adequate definition of geometrical acceptance. From the golden B decay, 88% of the leptons and 78% of the pions are within the geometrical acceptance, indicated in fig. 9 as dashed lines. The pions have a smaller acceptance because their mean momentum is lower than for the leptons, which results in a broadening of the polar angle distribution by the magnetic field.

4.4 Mean Efficiency

A display of an event[5] with seven superimposed interactions is shown in fig. 10. The lower part of this figure shows how the four tracks from the golden B decay are extracted by the pattern recognition algorithm. Figure 11 shows a closer look of the overlap section of inner and outer tracker. In fig. 12 only the detector

[5]all event displays have been produced with *prism 4.7* [6].

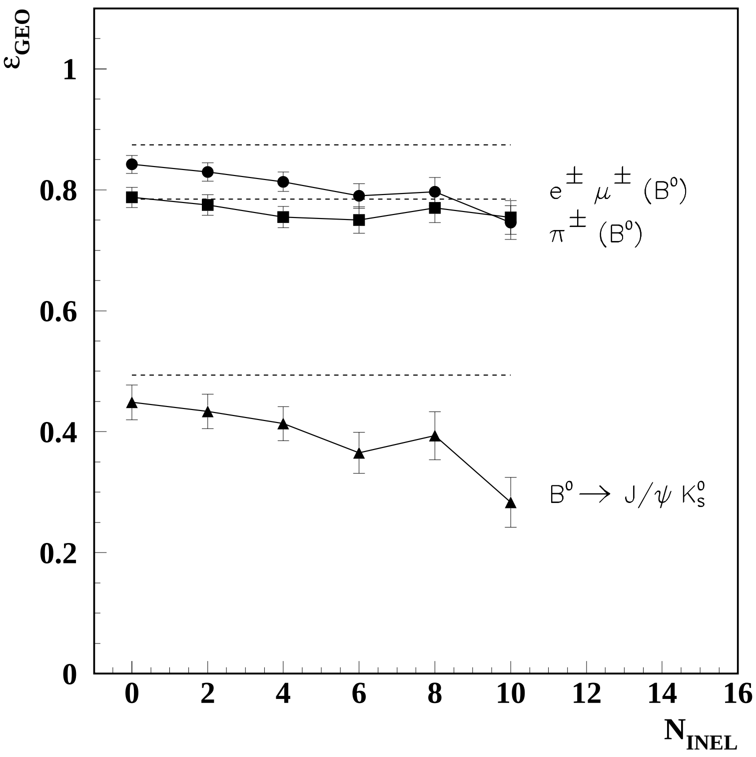

Figure 9: Fraction of particles related to the golden B decay satisfying the reference track criteria for different numbers of inelastic pileup interactions. The dashed lines show this fraction for $N_{\mathrm{Layers}} > 17$ for leptons (top) and pions (middle) from the golden B decay, and for the combination of all four daughters of the golden B decay (bottom). The solid symbols with error bars show the same fractions for $N_{\mathrm{Hits}} > 17$.

hits are displayed. The granularity of the tracker is still adequate in spite of the huge track density. Finally, fig. 13 shows an enlargement of the transition region between 5 mm and 10 mm cells in the outer tracker and demonstrates how left/right ambiguities and low momentum particles are handled by the algorithm.

The mean pattern recognition efficiencies for B interactions with on average four superimposed inelastic interactions (Poisson distributed) are shown in table 4. On average, 96.5% of the reference particles from the golden B decay are found. The mean efficiency for other charged particles is slightly smaller, which can be attributed to the larger track angles and smaller momenta as compared to the particles from the golden B decay. The ghost rate is smaller than 10%. The mean number of ghosts is 4.4 per event. Ghost rates of this level are uncritical because they are very likely to be removed in the subsequent magnet tracking step.

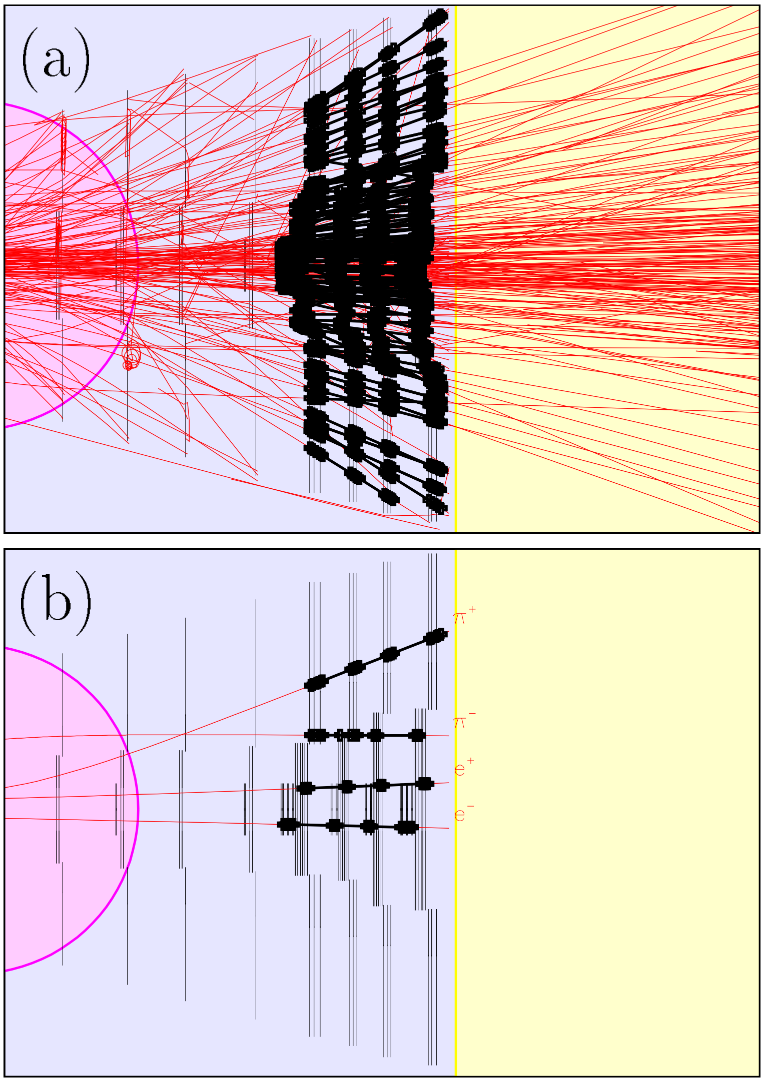

Figure 10: *prism* display of an event with seven superimposed interactions. The Monte Carlo tracks are shown as grey lines. The tracks found by the pattern recognition algorithm are shown as thick dark lines, with the hits used indicated by crosses. While (a) shows the whole event in the pattern tracker, in (b) the display is restricted to particles from the golden B decay.

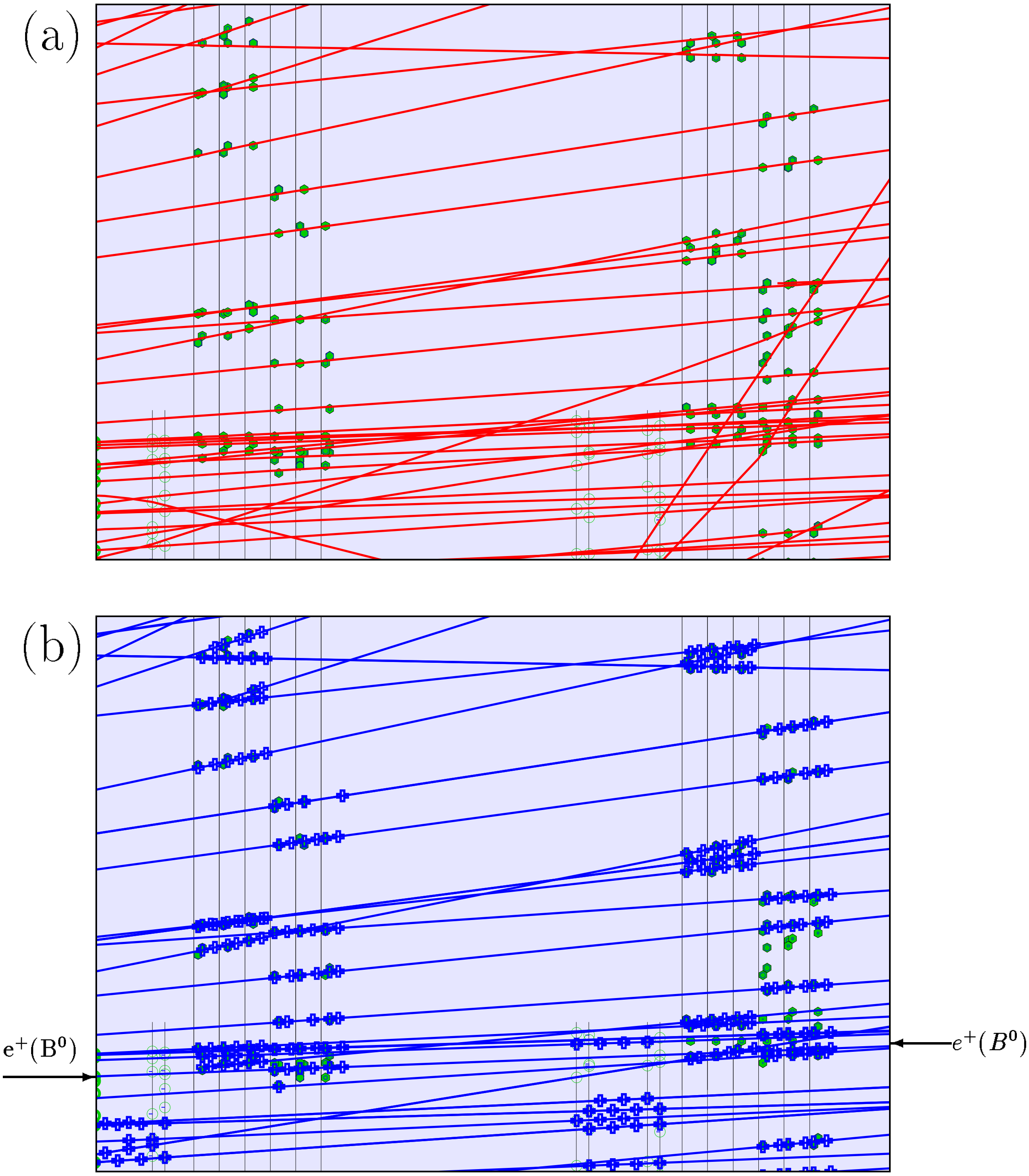

Figure 11: Closeups from the event in the previous figure, which contains seven superimposed interactions. Part (a) shows the Monte Carlo tracks with the digitized hits in the 0° projection, part (b) the hit pattern together with the reconstructed tracks. The fired honeycomb driftchamber cells are shown as hexagons and the inner tracker hits as circles. The crosses denote the reconstructed hit positions, also the hits obtained in the (otherwise invisible) stereo layers are shown.

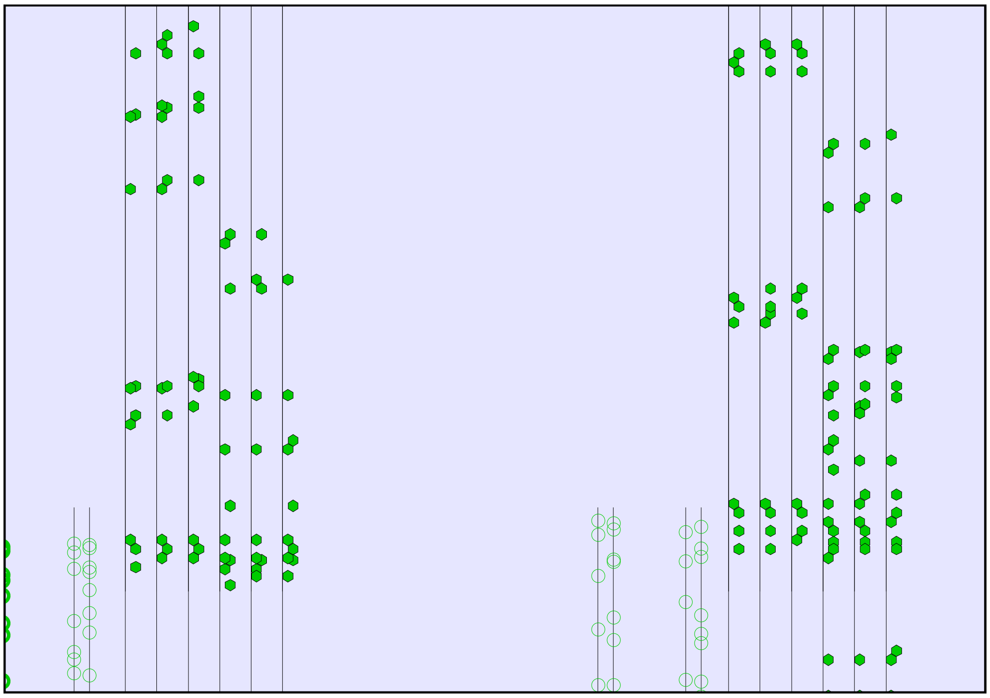

Figure 12: Same closeup as in the previous figure, showing only the detector hits. The fired honeycomb driftchamber cells are shown as hexagons and the inner tracker hits as circles. This view shows the adequacy of the HERA-B tracker granularity in spite of the huge track density for seven superimposed interactions.

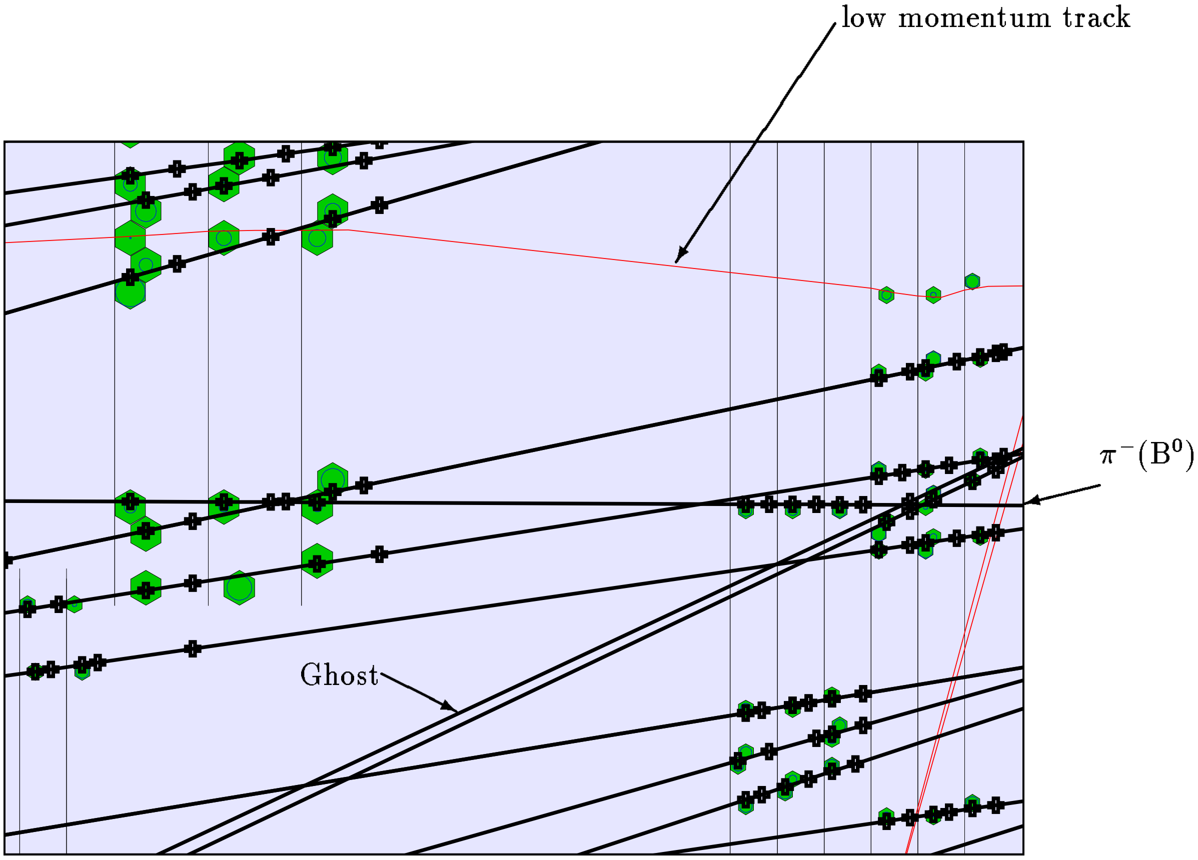

Figure 13: Closeup from the outer tracker section of the event in the previous figure. Inside the hexagonal honeycomb driftchamber cells, the drift-distance isochrones are indicated. Note the low-momentum track bent by multiple scattering in the upper part. A ghost track caused by left-right ambiguity is visible in the lower part.

Particle	ϵ $N_{Layers} > 17$	ϵ $N_{Hits} > 17$
$e^{\pm}_{J/\psi}$	$(95.3 \pm 1.3)\%$	$(98.8 \pm 0.7)\%$
$\mu^{\pm}_{J/\psi}$	$(96.4 \pm 1.2)\%$	$(98.3 \pm 0.8)\%$
$\pi^{\pm}_{K^0_S}$	$(97.3 \pm 0.8)\%$	$(98.0 \pm 0.6)\%$
$B^0 \to J/\psi K^0_S$	$(84.6 \pm 3.0)\%$	$(92.6 \pm 2.5)\%$
$X^{\pm}(p > 1$ GeV$)$	$(93.3 \pm 0.2)\%$	$(96.4 \pm 0.1)\%$
Ghosts	$(7.7 \pm 0.2)\%$	$(8.4 \pm 0.2)\%$

Table 4: Pattern recognition efficiencies for the main tracker

Note that the option of removing ghosts by means of a compatibility analysis has not been exploited yet.

Figure 14 shows the pattern recognition efficiency for different numbers of superimposed inelastic interactions. The efficiencies remain virtually at the same level up to $N_{INEL} = 6$. Even at $N_{INEL} = 8$, efficiencies and ghost rates are still at reasonable values.

The requirement of more than 17 traversed layers does not imply the presence of more than 17 Hits, since random hit inefficiencies and track overlaps might reduce the number of hits considerably. To investigate this effect, the reference track requirement was changed to $N_{Hits} > 17$. The resulting numbers, included in the right column of table 4 show that the efficiencies of the particles from the golden B decay are now above 98%. From a closer inspection of the small number of escaping particles, it was concluded that rare combinations of traversed planes which are not yet covered by the navigation tables are a main reason for the difference from unity in the pattern recognition efficiency.

The behaviour for different numbers of superimposed inelastic interactions (fig. 15) shows that the algorithm remains remarkably stable against increasing track density provided the number of hits on a track is sufficient. The number of particles fulfilling this criterion naturally decreases with increasing number of superimposed interactions, as can be seen in fig. 9. This effect is clearly related to track merging due to limited detector granularity.

4.5 Influence of Detector Efficiency

The mean efficiencies presented above have been calculated assuming a hit efficiency of 98% for the outer and 95% for the inner tracker devices. The first value has been verified in HERA-B test beam measurements with honeycomb drift chambers [15], the latter appears to be a safe assumption, e.g. for MSGCs. The influence of the detector efficiency was studied by varying this parameter in the digitization phase (fig. 16). Above $\epsilon_{HIT} = 95\%$, the hit inefficiency is well compensated by the algorithm (operating with $N_{Faults} = 2$), while smaller hit

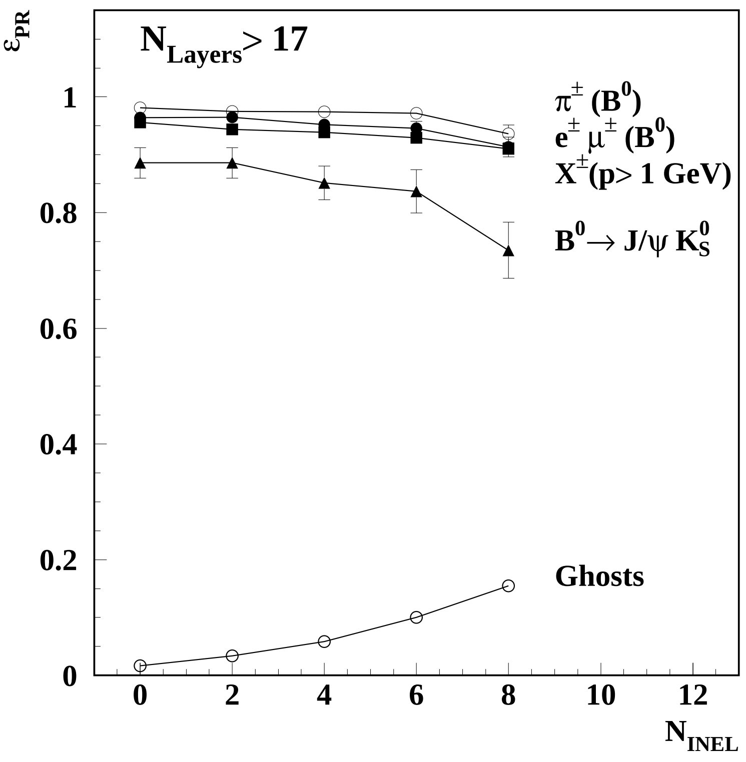

Figure 14: Pattern recognition efficiency versus number of inelastic interactions, which are superimposed on the interaction generating the B^0 ($\mathrm{N_{Layers}} > 17$). Note that since the same generated interactions have been combined with different pileup rates, correlations are visible in the statistical errors.

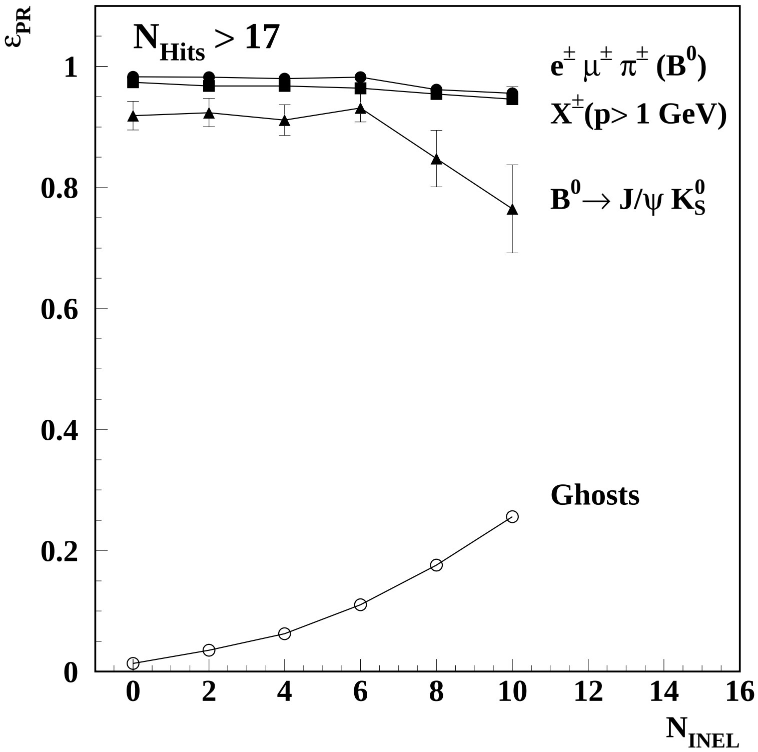

Figure 15: Pattern recognition efficiency versus number of inelastic interactions, which are superimposed on the interaction generating the B^0 ($N_{Hits} > 17$)

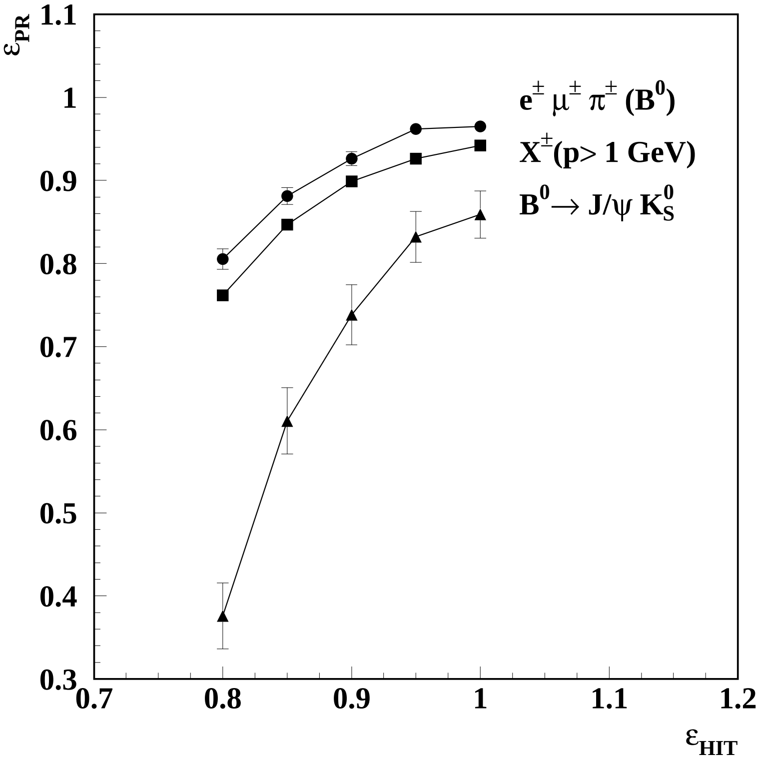

Figure 16: Pattern recognition efficiency for different values of the hit efficiency

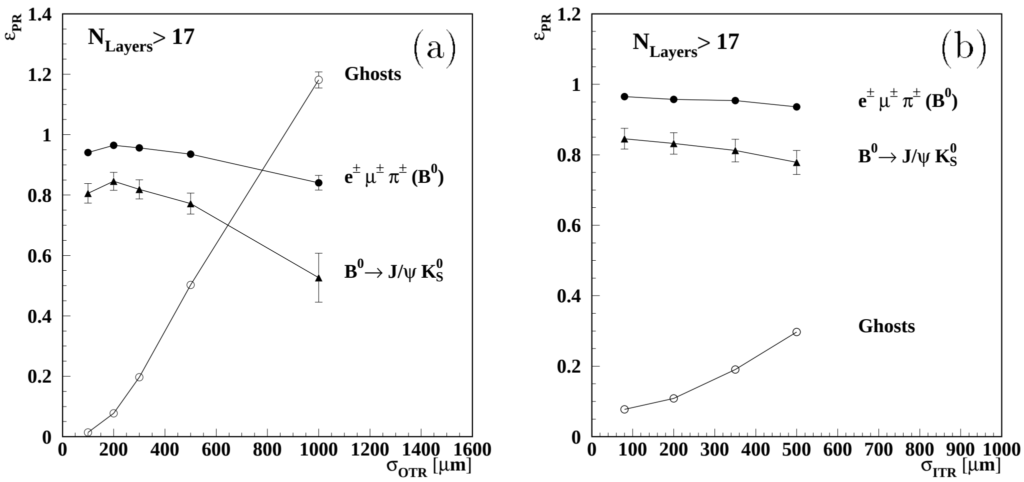

Figure 17: Pattern recognition efficiency for different outer (a) and inner tracker resolutions (b).

efficiency leads to sizeable loss in the fraction of detected particles from golden B decays.

4.6 Influence of Detector Resolution

The resolutions of outer and inner tracker modules were varied independently. Fig. 17a shows the influence of the outer tracker resolution. The efficiency degrades only slowly when the resolution is increased up to 1 mm. The effect that the efficiency drops again at 100 μm is artificial since the algorithm contains approximations related to the track angle which are no longer valid for $\sigma_{\rm OTR} \ll 200\ \mu$m. The detector resolution has an important impact on the ghost rate. A resolution worse by a factor of five yields more than a tenfold number of ghosts. It is also obvious that in the standard setup, almost all ghosts originate in the outer tracker.

Fig. 17b shows a similar investigation for the resolution of the inner tracker. The result shows that the efficiency hardly degrades for resolutions better than 200 μm. The impact of the inner tracker is here limited by the fact that 73% of the reference tracks are found in the outer tracker.

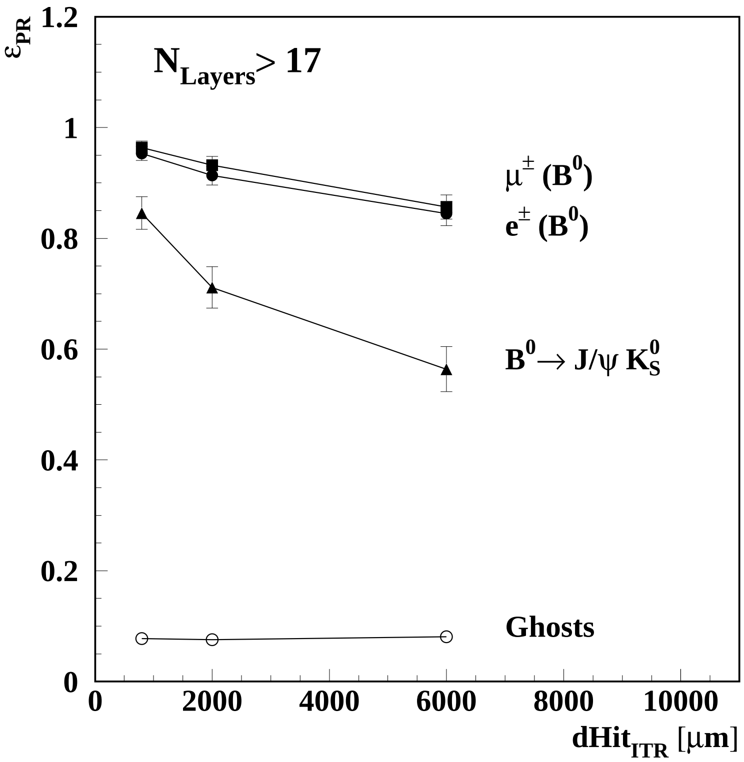

Figure 18: Pattern recognition efficiency for different double hit resolutions of the inner tracker.

4.7 Influence of Double Hit Resolution

An even more important parameter of the inner tracker digitization is the double hit resolution, i.e. the distance down to which the hits from nearby tracks can be resolved. As visible in fig. 18, the efficiency is reduced considerably if the double hit resolution is significantly worse than the standard value of 800 μm.

4.8 Track Parameters

For the efficiencies shown in the previous sections, a particle was regarded as properly reconstructed if it contributed more than 70% of all hits to a particular track candidate. It is important to verify that this *hit matching* criterion is applicable. This can be studied by investigating the track parameters of the track candidate. The *pull* of a track parameter $\mathcal{X}_i$ is defined by

$$\mathcal{P}(\mathcal{X}_i) = \frac{\mathcal{X}_i^{REC} - \mathcal{X}_i^{MC}}{\mathcal{C}_{ii}^{1/2}}$$

where $\mathcal{X}_i^{REC}$ is the reconstructed track parameter and $\mathcal{X}_i^{MC}$ the corresponding Monte Carlo value, while $\mathcal{C}_{ii}$ is the estimate for the corresponding covariance matrix diagonal element. Figure 19 shows the pulls for the four track parameters x, y, t_x and t_y for track candidates assigned to a particle from the golden B decay in comparison to the results of an *idealized* pattern recognition where the proper hits have been selected using Monte Carlo information. While the fitted widths agree with unity in the latter case, the pulls for the tracks from real pattern recognition are typically 30% wider. This can be attributed to inevitable unresolved left/right ambiguities, hits picked up from other, intersecting tracks and a simplified (and faster) treatment of multiple scattering compared to the full track fit. The important observation is however that there are no tails in the parameter distributions which might be harmful to a proper continuation of segments through the magnet.

4.9 Speed

The HERA-B experiment will process the events *quasi-online* on a scalable processor farm [16, 17]. The number of simultaneous interactions in one recorded event will have a wide distribution, the exact shape of which is determined by the beam particle flow through the target and the combined action of the trigger levels. For the implementation of a track reconstruction application on a processor farm, the good behaviour of the algorithm for high interaction multiplicities is essential, since e.g. an exponential rise of the computing time per event – as suggested by combinatorics – would tend to block farm nodes for an undue amount of time. Figure 20 shows the average computing time per event normal-

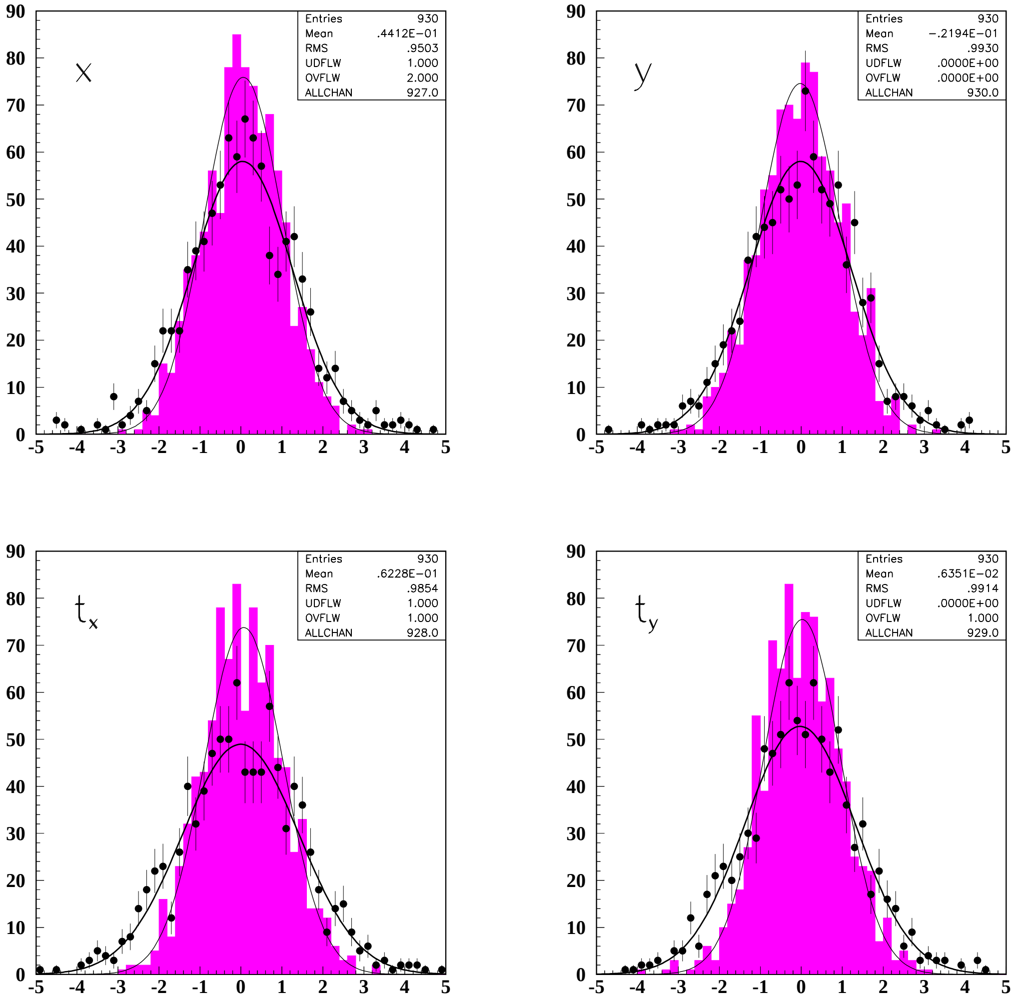

Figure 19: *Pulls* (for definition see text) of the four track parameters for ideal track reconstruction (shaded histogram) and real pattern recognition (points with error bars) for tracks from the golden B decay, both fitted with Gaussians. While the distributions for real pattern recognition are wider than for an ideal track fit, there is no indication of tails.

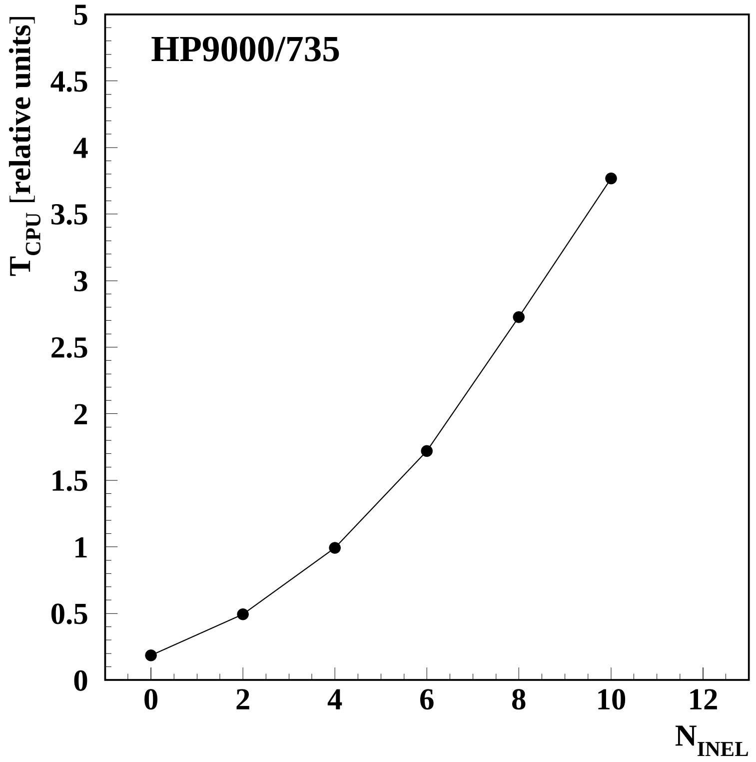

Figure 20: Mean computing time per event as a function of the number superimposed inelastic interactions, scaled to the value for the standard four superimposed interactions.

ized to that for the nominal four superimposed inelastic interactions[6]. After an initial nonlinear rise, the computing time per event settles on a linear dependence – indicating a constant amount of time per track – and is thus sufficiently well-behaved for an implementation on a processor farm.

5 Summary

A comprehensive technique for pattern recognition in a multiplanar B spectrometer geometry has been developed for the HERA-B main tracking system. The *concurrent track evolution* strategy evaluates the *available paths* for a track candidate using the Kalman filter method, combining virtues of local and combinatorial pattern recognition methods. In a first pass, two-dimensional track finding in the 0° projection provides the first two track parameters, while the other two are determined in the second pass using the information of both stereo projections simultaneously. The method was implemented for the HERA-B *pattern tracker* and tested on FRITIOF/PYTHIA events passed through the full HERA-B detector simulation. The method yields high pattern recognition efficiencies ($\sim$ 96.5%) with a ghost rate below 10% for interactions containing B mesons with on average four superimposed inelastic interactions. The results show that the method gives reasonable results up to at least ten superimposed inelastic interactions. The effect of inner and outer tracker resolutions and hit efficiencies on the pattern recognition performance has been studied in detail, providing several constraints for the detector design in LHC-like tracking scenarios.

The concepts of *concurrent track evolution* and *domain navigation* are also very well suited for three-dimensional track propagation through the magnet tracker (with inhomogeneous field maps) and into the adjacent tracking detectors. The discussion of these applications is deferred to individual documents.

Acknowledgements

I am greatly indebted to Thomas Lohse for sharing with me his experience and insight in the field of track reconstruction. Cordial thanks also to Hartwig Albrecht and Siegmund Nowak for their help in using their HERA-B software tools for event handling (*Arte*) and simulation (*HBGEAN*). I would also like to thank Rudolf Frühwirth and Igor Gavrilenko for inspiring discussions about pattern recognition. The excellent operation of the computer systems at DESY-Zeuthen and at the EEL group of the Humboldt University in Berlin was an essential asset for these studies, and I would like to thank the staff of the Zeuthen computer

[6] In the current implementation, the average computing time for such an event was 4.4s on a HP9000/735 with a clock rate of 125 MHz. No particular acceleration techniques in the code have been exploited yet.

center and Olf Epler (Berlin) for their continuous help and support. This work was supported by the Bundesministerium für Bildung, Wissenschaft, Forschung und Technologie under contract number 05 7 BU 35I (5).

References

[1] T. Lohse et al., *An Experiment to Study CP Violation in the B System Using an Internal Target at the HERA Proton Ring* (Proposal), DESY-PRC 94/02 (1994).

[2] K. Kirsebom et al., *A Dedicated LHC Collider Beauty Experiment for Precision Measurements of CP Violation* (Letter of Intent), CERN/LHCC 95-5 (1995).

[3] E. Hartouni et al., *An Experiment to Study CP Violation in the B System Using an Internal Target at the HERA Proton Ring* (Design Report), DESY-PRC 95/01.

[4] C. Stegmann, Nucl. Instr. and Meth. A384 (1996) 196.

[5] J. Rieling, *Tracking in the Silicon*, HERA-B Note 95-068 (1995). `http://www-hera-b.desy.de/subgroup/software/susi.ps`

[6] R. Mankel, *prism – the HERA-B Event Display*, HERA-B Note 95-128 (1995). `http://www-hera-b.desy.de/subgroup/software/prism.ps`

[7] R. Mankel, *Pattern Recognition Algorithms for B Meson Reconstruction in Hadronic Collisions*, Contributed paper to the CHEP conference Berlin 1997, to be published in Comp. Phys. Comm.

[8] M. Regler, R. Frühwirth and W. Mitaroff, Int. Journ. Mod. Phys. C7 (1996) 521.

[9] R.E. Kalman, Trans. ASME, J. Basic Engineering (1960);
R. Battin, Am. Rocket Soc. 32 (1962) 1681;
R.E. Kalman and R.S. Bucy, Trans. ASME, J. Basic Engineering (1962);
R. Frühwirth, Nuclear Instr. and Meth. A262 (1987) 444.

[10] P. Billoir and S. Qian, Nuclear Instr. and Meth. A294 (1990) 219.

[11] R. Mankel, *Application of the Kalman Filter Technique in the HERA-B Track Reconstruction*, HERA-B Note 95-239 (1995). `http://www-hera-b.desy.de/subgroup/software/kalman-filter.ps`

[12] H. Albrecht et al., *ARTE. The Event Reconstruction and Analysis Tool for HERA-B*, HERA-B Internal note (1996). `http://www-hera-b.desy.de/subgroup/software/arte/arte_manual.ps`

[13] T.S. Sjöstrand, CERN-TH-6488-92 (1992);
B. Anderson, G. Gustafson and Hong Pi, Z. Phys. C57 (1993) 485.

[14] S. Nowak, *HBGEAN and HBRCAN*, HERA-B Internal Note (1995). `http://www-hera-b.desy.de/subgroup/software/hbgean.html`

[15] H. Deckers et al., *Beam Tests of Honeycomb Drift Chambers*, HERA-B note in preparation.

[16] R. Mankel, Nucl. Instr. and Meth. A384 (1996) 201.

[17] A. Gellrich et al., *The Processor Farm on Online Triggering and Full Event Reconstruction of the HERA-B Experiment at HERA*, HERA-B Note 95-147 (1995).